ORGANIC CHEMISTRY

Regiodivergent catalytic asymmetric dearomative cycloaddition of bicyclic heteroaromatics

Lei Peng[1]†, Zhen Zeng[2]†, Kai Li[1], Yidong Liu[1], Yu Lan[2,3]*, Hailong Yan[1]*

The catalytic dearomative cycloaddition of bicyclic heteroaromatics including benzofurans and indoles provides rapid access to functionalized heterocyclic molecules. Because of the inherent stereoelectronic differences, the furan or pyrrole nucleus is more prone to dearomative cycloaddition than the benzene ring. Here, we realized a geometry-based differentiation approach for achieving C6-C7 and C7-C7a regioselectivity. The rotationally restricted σ bond at C7 position respectively placed the C6-C7 and C7-C7a sites of benzofurans or indoles in an optimal spatial orientation toward the axially chiral heterodiene, thus affording two enantioenriched polycyclic compounds from a single racemic heterobiaryl atropisomers. Calculation results of density functional theory interpreted the mechanism of this parallel kinetic resolution. The bioactivity of the dearomatized products was evaluated in cancer cell lines with certain compounds exhibiting interesting biological activities.

INTRODUCTION

Catalytic asymmetric dearomative cycloaddition represents an ideal strategy of converting the readily available aromatics into cyclic molecules with multiple stereocenters which are of increasing interest in medicinal chemistry and nature product synthesis (1, 2). Despite the tremendous advances in this field, achieving the regio- and stereoselectivity of the catalytic asymmetric dearomative cycloaddition reactions remains a challenge (3–5) due to the harsh reaction conditions required for breaking the aromaticity and the insufficient stereoelectronic differences among the latent alkene subunits of the aromatics (6–8). These obstacles prevent the development of catalytic asymmetric dearomative cycloaddition with a broad scope.

Benzofurans and indoles, bicyclic benzoheteroaromatics, are prone to the catalytic asymmetric dearomatization reactions (9–12) due to their reduced resonance stabilization energy (13–20). The catalytic asymmetric dearomative cycloaddition of benzofuran or indole derivatives typically occurs at C2-C3 site (Fig. 1A) (21–26). The excellent regioselectivity is rationalized by the inherent electron-rich property and restoration of the aromaticity in the benzene ring during cycloaddition. However, a common problem encountered in chemical synthesis is how to access the dearomative cycloaddition of the benzene ring in benzofurans and indoles. As depicted in Fig. 1B, the heat of hydrogenation of alkenes in benzofuran cleanly demonstrates that the disruption of the aromaticity of benzene ring is thermodynamically unfavorable (C6-C7), even more so with simultaneously disturbing the aromaticity of the two consecutive aromatic rings (C7-C7a) (27, 28). To the best of our knowledge, regio- and stereoselectivity cycloaddition of benzofurans and indoles at C6-C7 and C7-C7a sites have never been achieved.

Atropisomers feature a conformationally restrained stereogenic axis with a sufficiently large rotational barrier that leads to a stable configuration and spatial separation of the flanking substituents (29–32). Thus, controlling the configuration of the atropisomers would result in the predictable geometric orientation of the functionalities in the pivoting units about the stereogenic axis. This unique nature of atropisomers enables the geometry-based differentiation between C6-C7 and C7-C7a sites of benzofurans and indoles if a stereogenic axis is established at the C7 position to form heterobiaryl atropisomers. Our design was introducing an axially chiral vinylidene ortho-quinone methide (33) (VQM) fragment as an ortho-substituent next to the axis into the aromatic ring. The in situ generation of rigid VQM under catalyst control would place the reactive heterodiene motif of VQM out of plane of the aromatic ring, thus in close proximity to a single target C6-C7 or C7-C7a site (Fig. 1C, paths a and b). The large driving force for VQM rearomatization and the lowered entropic barriers would lead to regioselective disruption of the aromaticity of benzene ring in benzofurans or indoles. Enantioselectivity was enforced through efficient axial-to-central chirality transfer during the cycloaddition. Overall, the racemic heterobiaryl atropisomers containing benzofuran or indole segments enables the access to two enantioenriched products each (Fig. 1C, bottom), thus resulting in a parallel kinetic resolution (PKR) (34–38). This protocol rapidly increases the structural complexity of benzofuran and indole dearomatization products and paves an avenue to medicinally relevant heterocycles.

RESULTS AND DISCUSSION

Preliminary validation

First, 1-ethynylnaphthalen-2-ol derivative **1af** featuring a benzofuran motif was treated with N-bromosuccinimide (NBS) in the presence of 20 mole percent (mol %) quinine-derived amide catalyst **C** (39–43) in toluene at −40°C. Axially chiral product **2af** was obtained without dearomatized heterocyclic compounds. This result might be attributed to the competing conjugate addition of aryl nucleophile to VQM intermediate. The subsequent elimination-rearomatization sequence under basic reaction conditions led to the axially chiral biaryl **2af**. To suppress the formation of axially

[1]Chongqing Key Laboratory of Natural Product Synthesis and Drug Research, Chemical Biology Research Center, School of Pharmaceutical Sciences, Chongqing University, Chongqing, China. [2]Chongqing Key Laboratory of Theoretical and Computational Chemistry, School of Chemistry and Chemical Engineering, Chongqing University, Chongqing, China. [3]Green Catalysis Center, College of Chemistry, Zhengzhou University, Zhengzhou, China.
*Corresponding author. Email: lanyu@cqu.edu.cn (Y.La.); yhl198151@cqu.edu.cn (H.Y.)
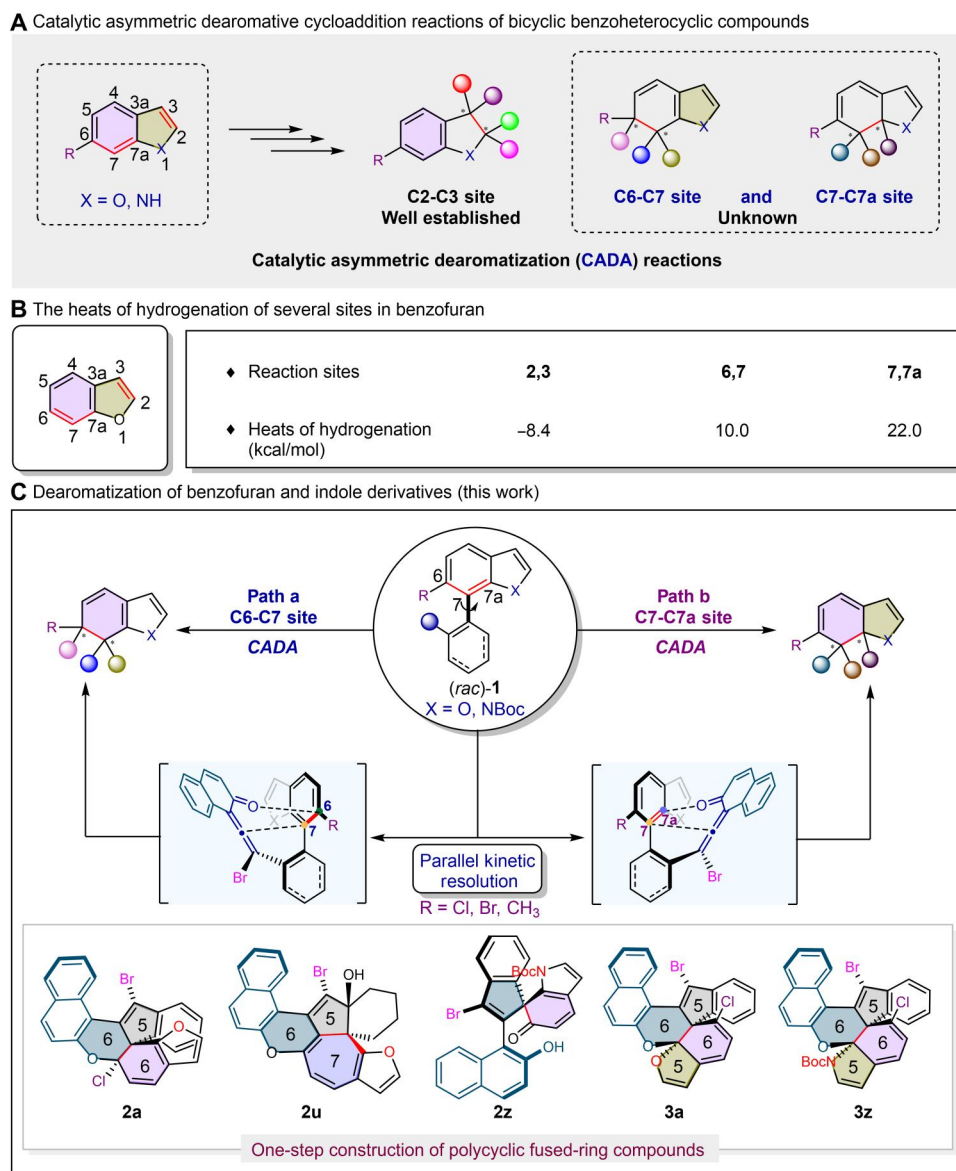†These authors contributed equally to this work.

Fig. 1. Background and reaction development. (**A**) The selectivity challenges in catalytic asymmetric dearomatization of bicyclic heteroaromatics. (**B**) The heats of hydrogenation of several sites in benzofuran. (**C**) This work: Regiodivergent catalytic asymmetric dearomative cycloaddition of bicyclic heteroaromatics at C6-C7 and C7-C7a sites.
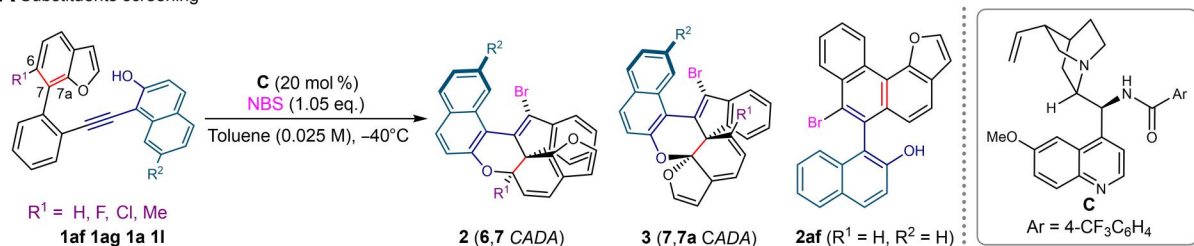
product **2af**, a fluorine was introduced at the C6 site of the benzo-furan motif to stabilize the carbon-fluorine bond rehybridization during the cycloaddition. Gratifyingly, dearomatized cycloadducts **2ag** and **3ag** were readily formed in high yields and excellent stereo-selectivities. The moderate regioselectivity (4.8:1) in favor of **2ag** il-lustrated that C6-C7 site of benzofuran was more reactive than C7-C7a site. When the σ bond at C7 site rotated freely, the VQM inter-mediate could discriminate the C6-C7 site from C7-C7a site, thus resulting in preferential reaction at C6-C7 site. If the rotation of the σ bond at C7 site was hampered, then the regioselectivity could be enforced. Thus, the bulky substituents, including chloride and methyl, were evaluated at C6 site. Both regiomers **2** and **3** were gen-erated in comparable yields. The chemical structures and absolute configurations of **2g**, **2l**, **2af**, **2ag**, and **3h** were confirmed by x-ray

crystallography (Fig. 2A). In addition, the optically pure atropisom-ers (*R*)-**1p** and (*S*)-**1p** were synthesized and subjected to the asym-metric dearomative cycloaddition reaction, respectively. These control experiments exhibited high specificity. (*R*)-**1p** generated the regiomer **2p′** (C6-C7 regioselectivity) as the exclusive product, whereas (*S*)-**1p** yielded the regiomer **3p′** (C7-C7a regioselectivity) (Fig. 2B). The absolute configurations of (*R*)-**1p** and (*S*)-**1p** were determined by circular dichroism spectroscopy (see the Supple-mentary Materials).
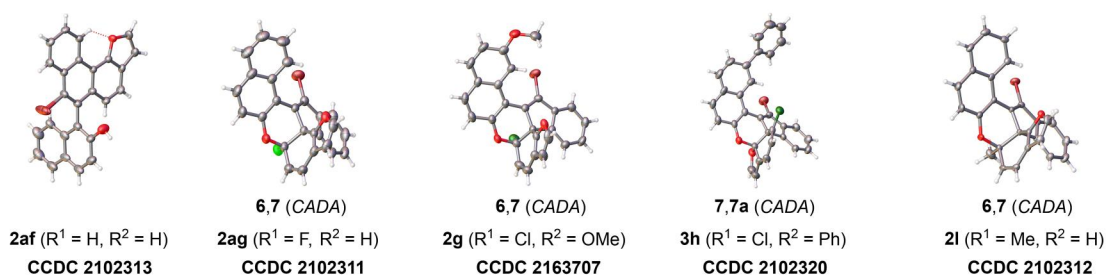
Mechanistic study

Density functional theory (DFT) calculations were used to reveal the mechanism of PKR for the formation of different chiral regiom-ers. In our theoretical calculations (Fig. 3), racemic 1-
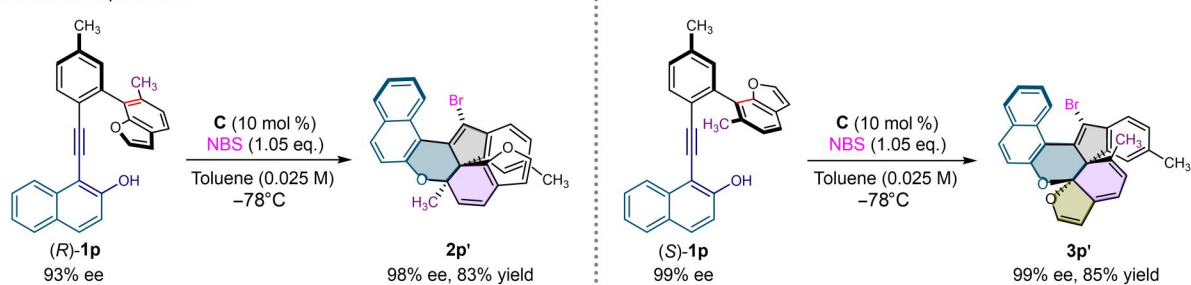
Fig. 2. Substituents screening and control experiments. (**A**) Substrates **1af**, **1ag**, **1a**, **1l** (0.05 mmol), and catalyst **C** (20 mol %) in toluene (2.0 ml) at −40°C for 15 min and then NBS (1.05 equiv.) at −40°C, 8 hours. Isolated yield. The ee values were determined by high-performance liquid chromatography (HPLC) analysis with a chiral stationary phase. The diastereomeric ratio (d.r.) was determined by ^{1}H nuclear magnetic resonance (NMR) analysis of the crude mixtures. n.d., not detected. (**B**) Substrates (*R*)-**1p**, (*S*)-**1p** (0.05 mmol), and catalyst **C** (10 mol %) in toluene (2.0 ml) at −78°C for 15 min and then NBS (1.05 equiv.) at −78°C, 12 hours.

ethynylnaphthalen-2-ol derivative **1a** was chosen as the model reactant. In this molecule, two potential stereogenic axes were found in biaryl and diaryl alkyne moieties, respectively, which would result to four possible atropisomers, namely, (**1aS,2aR**)-**1a**, (**1aR,2aR**)-**1a**, (**1aS,2aS**)-**1a**, and (**1aR,2aS**)-**1a**. DFT calculation results clearly revealed that the rotation of the axis of diaryl alkyne was almost barrierless, because the triple bond of alkyne reduced the restraint of the two terminal aryl groups. Therefore, it was easy to realize the isomerization between (**1aS,2aR**)-**1a** and (**1aS,2aS**)-**1a**. However,

the calculated activation free energy for the rotation of biaryl's axis was as high as 29.5 kcal/mol, which indicated a restrained stereogenic axis leading to atropisomers with stable configurations. On the basis of this idea, we considered the reaction mechanisms of (**1aS,2aR**)-**1a**, (**1aR,2aR**)-**1a** individually. When **aS-1a** was used as the reactant, a three-component concerted deprotonation-bromination occurred in the presence of quinine-derived amide catalyst **C** via the transition state **2-ts-S**. In this transition state, the quinuclidine moiety of catalyst **C** acted as Brønsted base to
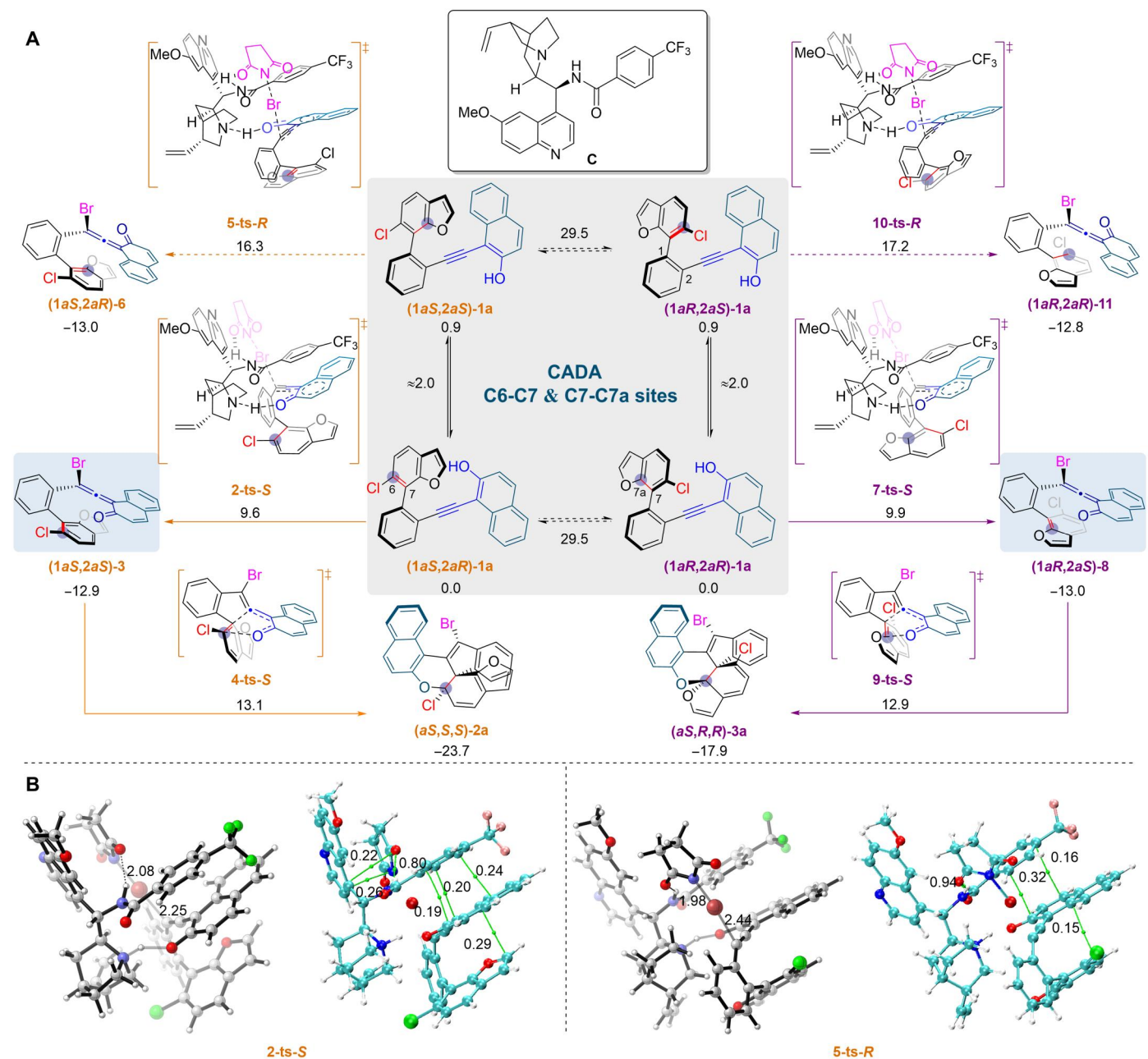
Fig. 3. DFT-computed Gibbs free energy changes of regiodivergent catalytic asymmetric dearomative cycloaddition of benzofuran. (**A**) All energies were calculated at a M06-2X/6-311 + G(d,p)/SMD(toluene)//M06-2X/def2-SVP/SMD(toluene) level of theory. Values are given in kcal/mol. (**B**) Structure information and Atoms-in-Molecules (AIM) analyses of **2-ts-S** and **5-ts-R**. Laplacian electron density values ($\nabla^2\rho$, *10^{-1} arbitrary units) at the bond critical points. The bond distances are in angstroms.

achieve deprotonation of the naphthalenol moiety of substrate **1a**. Meanwhile, the bromine atom was transferred from NBS to alkyne moiety in substrate **1a**. Moreover, a hydrogen bond between the amide moiety in catalyst **C** and succinimide could further stabilize the present transition state. The geometric information of transition state **2-ts-S** is given in Fig. 3B, where the diaryl alkyne moiety was set to be perpendicular to the page, and the hydroxyl group in naphthalenol moiety was defined as upward. The left side of substrate **1a** was blocked by benzofuranyl group, so the bromination occurred at

the right site of diaryl alkyne moiety. The quinuclidine moiety in catalyst **C** should be located on the upper side to achieve deprotonation, which was far away from the horizontal phenyl group in substrate **1a**. In this case, the N—H bond of amide moiety points to the back of the page, which could form a hydrogen bond with reacting NBS without strain. Meanwhile, a π-π stacking interaction was observed between succinimide and quinolyl group in catalyst **C**. The combination of these effects leads to a low activation free energy of only 9.6 kcal/mol for the concerted deprotonation-

bromination via transition state **2-ts-S**. After this step, an *S*-config-uration allene frame was formed in VQM intermediate (**1aS,2aS**)-**3**, where the chiralities of both allene's and biaryl's axes were locked. In intermediate (**1aS,2aS**)-**3**, the carbonyl group in VQM moiety was closed to C6 site of benzofuranyl. Therefore, the subsequent in-tramolecular [4 + 2] hetero-Diels-Alder cycloaddition via transition state **4-ts-S** could yield (**aS,S,S**)-**2a** as the major product. In contrast, the diastereomeric VQM intermediate (**1aS,2aR**)-**6** was formed by deprotonation-bromination of (**1aS,2aS**)-**1a** via transition state **5-ts-R** in the presence of catalyst **C** and NBS. The geometric informa-tion of **5-ts-R** is given in Fig. 3B, where the hydroxyl group in the naphthalenol moiety was changed as downward. In this case, the left side of substrate **1a** was also blocked by the benzofuranyl group. However, the steric repulsion was observed between the coming quinuclidine moiety in catalyst **C** and the horizontal phenyl group in substrate because the inherent chirality of quinine did not match that of the substrate. Moreover, the hydrogen bond between amide moiety in catalyst **C** and reacting NBS causes the succinimide to be parallel to the quinolyl group, thus destroying the π-π stacking interaction mentioned in **2-ts-S**. These factors work together to make the relative free energy of transition state **5-ts-R** higher than that of **2-ts-S** by 6.7 kcal/mol. When **aS-1a** was used as the substrate, (**aS,S,S**)-**2a** was found as the major product. The computational result fully agree with experimental ob-servations. In this case, we found that the benzofuranyl group only acted as a wall to block the left side of the alkyne moiety. Therefore, we assumed that the axial chirality of biaryl did not affect that of allene in VQM intermediate produced after alkyne bromination. As shown in Fig. 3A, when enantiomer **aR-1a** was selected as the substrate, a concerted deprotonation-bromination transition state **7-ts-S** was located, and its geometry was closed to that of **2-ts-S**. The only difference in **7-ts-S** is the benzofuranyl group is upward. The calculated activation free energy of this process via transition state **7-ts-S** was 9.9 kcal/mol and closed to that of the corresponding process via **2-ts-S**, indicating that the orientation of benzofuranyl did not affect the diastereoselectivity for the formation of allene in VQM intermediate by deprotonation-bromination. When VQM intermediate (**1aR,2aS**)-**8** was formed, the carbonyl group in VQM moiety was closed to C7a site of the benzofuranyl group. Therefore, the subsequent intramolecular [4 + 2] hetero-Diels-Alder cycloaddition via transition state **9-ts-S** yielded (**aS,R,R**)-**3a** as the major product. This result explains why two products with different regioselectivities can be obtained by PKR.

Substrate scope of the catalytic asymmetric dearomative cycloaddition of bicyclic heteroaromatics

Furthermore, the substrate scope was examined after a systemic re-action conditions screening (see the Supplementary Materials). In respect to the axially chiral benzofuran-based biaryls (**1b-1t**), various substituents including ethyl, propyl, cyclohexyl, and phenyl at the 6-position of the naphthol motif (**1b-1e**) were first ex-plored, providing the chiral polycyclic **2b-2e** and **3b-3e** in high yields and high to excellent enantioselectivities (Fig. 4A). Propyl, methoxyl, and phenyl groups at 7-position of the naphthol motif were accommodated to yield products **2f-2h** and **3f-3h**. Moreover, benzofurans **1i-1k** with methyl, methoxyl, or fluorine on ring A also successfully afforded the products **2i-2k** and **3i-3k**. When the chlo-ride at the 6-position of benzofuran was replaced by a methyl, the reactions proceeded smoothly to yield **2l-2t** and **3l-3t**. Delightedly,

the ring A could be replaced by a less conformationally restricted cyclohexene to afford the corresponding products **2u-2y** and **3u-3y**, in which **2u-2y** featuring [7-6-5] tricyclic system was assumed to be formed through the C6-C7 regioselective dearomative cyclo-additon followed by an unexpected ring expansion (Fig. 4B). In ad-dition, the operationally simple conditions with subtle modifications could be extended to axially chiral indole-based biaryls (see the Supplementary Materials). Racemic **1z-1ae** under-went dearomatization smoothly and therefore furnished the prod-ucts **2z-2ae** and **3z-3ae** (Fig. 4C). The construction of unexpected spiro-cyclic compounds **2z-2ae** was believed to proceed through C6-C7 regioselective dearomative cycloaddition and subsequent hydrolysis. The structures and absolute configurations of the prod-ucts **2g**, **2l**, **2v**, **2aa**, **3h**, **3y**, and **3ae** were determined by x-ray crys-tallography, and the configurations of other products in Fig. 4 were assigned by analogy.

Anticancer activity test

We further investigated the potential applications of the new syn-thetic compounds without further modifications for medicinal pur-poses. The in vitro screening on a small panel of cancer cell lines including A549, Hela, MIA PaCa-2, MCF-7, CT26, B16F10, A375, and MDA-MB-231 was performed with the final products, and compound **3ae** exhibited the better antiproliferation activity than other products (Fig. 5A). Especially, it inhibited A375 cells with a median inhibitory concentration (IC_{50}) value of 7.68 μM, while its cytotoxicity toward noncancer cells L02 was minimal ($IC_{50} > 100$ μM). In addition, the immunofluorescence assay on A375 cells indicated that **3ae** could induce morphological alter-ations, which became more pronounced when the concentration range of **3ae** was expanded up to 20 μM (Fig. 5B). Concisely, a reduced density of cells, a decreased mitochondrial compactness (red staining), and remarkably altered cytoskeletons (green stain-ing) were observed in treated groups, but the shape of the nucleus (blue staining) only changed slightly (fig. S24). These morphologi-cal changes indicated that **3ae** markedly disrupted mitochondria or-ganization and might eventually lead to cell apoptosis. Given the interesting profile of **3ae**, we carried out flow cytometric assays to explore its functional mechanisms. Compound **3ae** could induce apoptosis in A375 cells (Fig. 5C), and the percentages of total apo-ptotic cells increased dose-dependently (1.9, 9.6, 12.8, and 24.5%, corresponding to 0, 8, 16, and 24 μM **3ae**). Meanwhile, notable in-duction effect of **3ae** on cell cycle arrest was observed, and the per-centage of the cells in the G_0/G_1 period increased from 39.1 to 54.8% after the cells were treated by 24 μM **3ae** (Fig. 5D). This finding sug-gested that **3ae** might exerted its antiproliferation activity via the cell cycle mechanism. Hence, we searched for cell cycle–related biomol-ecules from literature and retrieved their crystal structures from the Protein Data Bank (PDB) database. Reverse docking results suggest-ed that the human DNA topoisomerase I was among the top poten-tial targets. Compound **3ae** could insert into the known camptothecin binding site (Fig. 5E) and bind to the target via a hy-drogen bond and other noncovalent interactions (fig. S25). After-ward, this intention was validated by DNA electrophoresis assays (Fig. 5F), and **3ae** inhibited the enzymatic activity of DNA topo-isomerase I dose-dependently. Overall, **3ae** exhibited impressive bi-ological activities and might be further developed for medicinal applications.
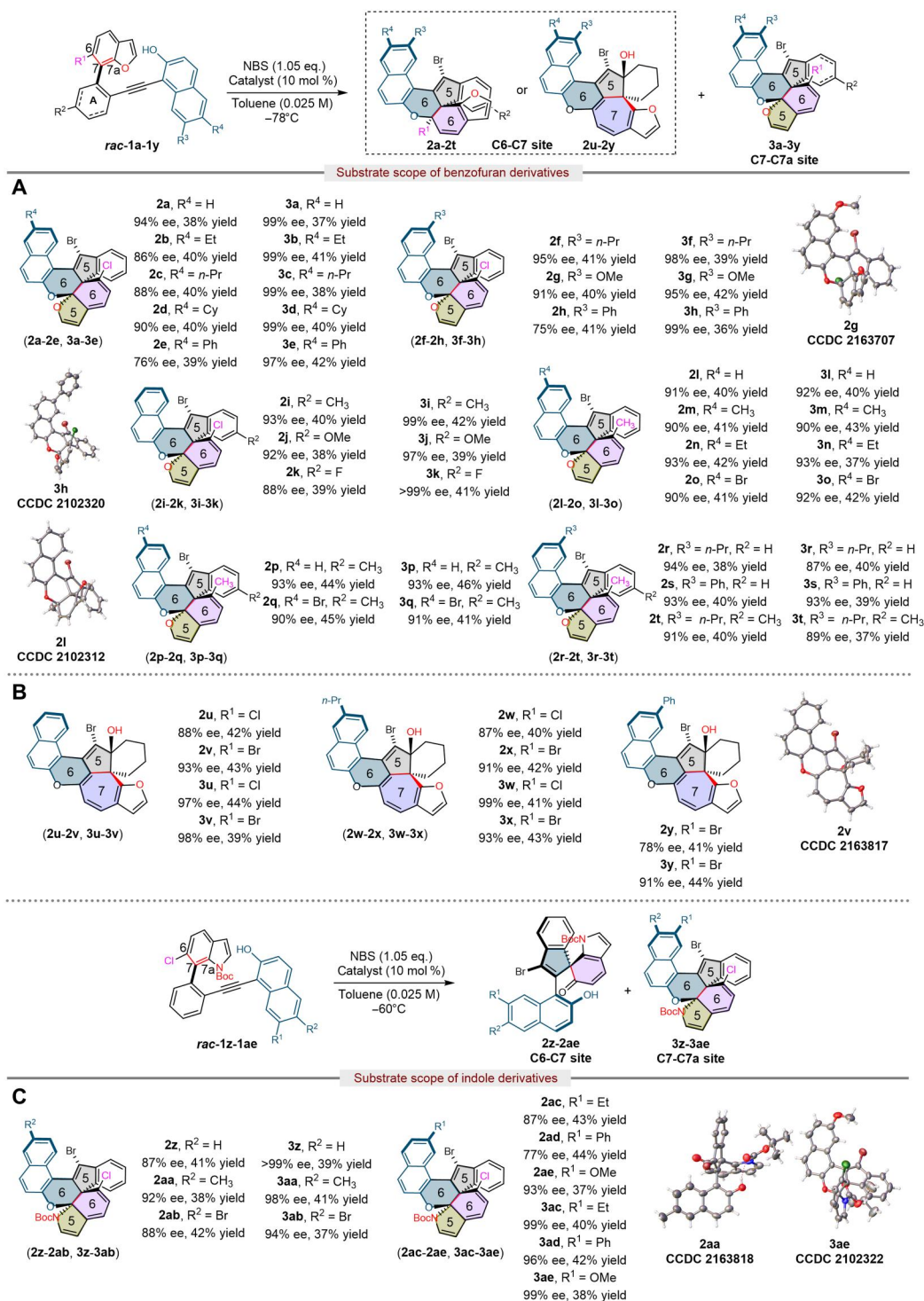
Fig. 4. Scope of the catalytic asymmetric dearomative cycloaddition of bicyclic heteroaromatics. Reaction conditions: (**A**) Substrates **1a-1t** (0.15 mmol) and catalyst **C** (10 mol %) in toluene (6.0 ml) at −78°C for 15 min and then NBS (1.05 equiv.) at −78°C, 12 hours. Isolated yield. The ee values were determined by HPLC analysis with a chiral stationary phase. (**B**) Substrates **1u-1y** (0.15 mmol) and catalyst **I** (10 mol %) in toluene (6.0 ml) at −78°C for 15 min and then NBS (1.05 equiv.) at −78°C, 24 hours. (**C**) Substrates **1z-1ae** (0.15 mmol) and catalyst **I** (10 mol %) in toluene (6.0 ml) at −60°C for 15 min and then NBS (1.05 equiv.) at −60°C, 12 hours.
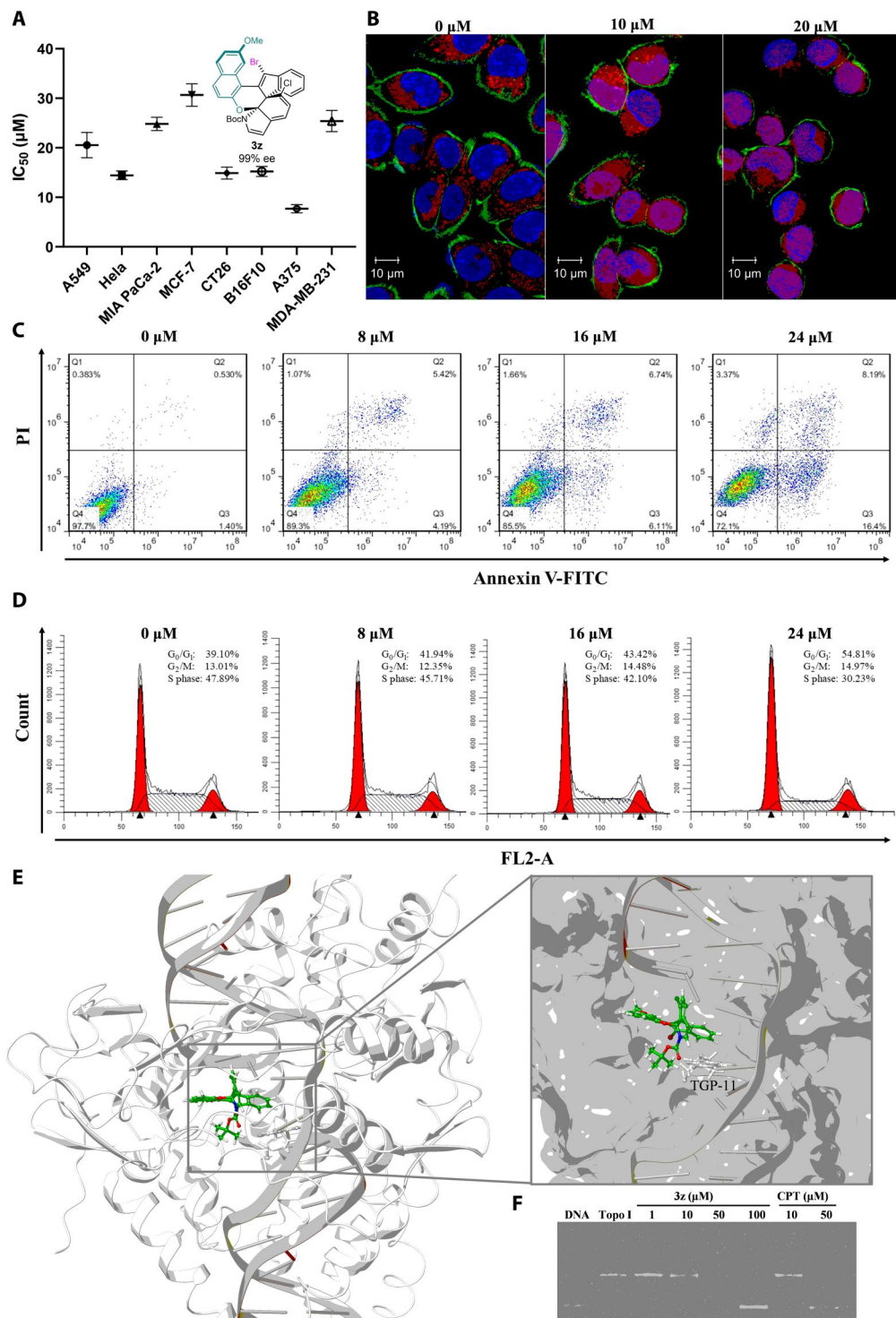
Fig. 5. Pharmacological profile of 3ae. (**A**) IC$_{50}$ values of **3ae** against a panel of cancer cell lines measured by 3-(4,5-Dimethylthiazol-2-yl)-2,5-diphenyltetrazolium bromide (MTT) assay. Data are presented as the mean ± SD from three independent experiments. (**B**) Morphologic alterations of A375 cells treated by **3ae** (0, 10, and 20 μM) for 24 hours. (**C**) A375 cells apoptosis induced by **3ae** (0, 8, 16, and 24 μM) for 24 hours. PI, Propidium Iodide. (**D**) A375 cell cycle arrest induced by **3ae** (0, 8, 16, and 24 μM) for 24 hours. (**E**) Molecular docking of **3ae** with DNA topoisomerase I (PDB code: 1SC7). For the sake of clarity, proteins were represented in gray ribbons and surfaces. (**F**) Effect of **3ae** on the relaxation of supercoiled pBR322 DNA mediated by DNA topoisomerase I (Topo I).

In summary, we have developed a regiodivergent catalytic asymmetric dearomative cycloaddition protocol of benzofurans and indoles. In the protocol, the reactive site at C2-C3 could be circumvented to achieve C6-C7 and C7-C7a regioselectivity, which could disrupt the aromaticity of benzene ring or even simultaneously disturbed the aromaticity of the two consecutive aromatic rings. This methodology markedly increased the structural complexity of benzofuran and indole dearomatization products. The control experiments and theoretical studies provided the evidence for the regiodivergent PKR. Given that the benzofuran- and indole-based polycyclic are privileged structures in drug discovery, we also showed the dearomatived product **3ae** has anticancer activities.

MATERIALS AND METHODS

All of the reagents were purchased from commercial suppliers and used without further purification unless otherwise noted. The ^{1}H nuclear magnetic resonance (NMR) and ^{13}C NMR spectra were obtained with an Agilent 400MR or 600MR DD2 spectrometer at ambient temperature. Electrospray ionization–high-resolution mass spectrometry was performed with a Bruker Solari X 7.0 T spectrometer or H2Os SYNAPT G2 spectrometer. X-ray crystallography analysis of the single crystals was performed with an Agilent SuperNova-CCD x-ray diffractometer.

General procedure for the preparation of racemic 2a-2ag and 3a-3ag

A solution of *rac*-**1a**-**1ag** (0.025 mmol, 1.0 equiv.) in toluene (1.0 ml) was stirred at −30°C for 15 min, and then NBS (1.05 equiv.) was added. The reaction mixture was stirred at −30°C and monitored by thin-layer chromatography (TLC). After completion of the reaction, the mixture was purified by preparative TLC on silica gel to yield the target molecular racemic compounds.

General procedure for the catalytic PKR of racemic 1a-1t

A solution of *rac*-**1a**-**1t** (0.15 mmol, 1.0 equiv.) and catalyst **C** (10 mol %) in toluene (6.0 ml) was stirred at −78°C for 15 min, and then NBS (1.05 equiv.) was added. After stirring at −78°C for 12 hours, the mixture was subjected to silica gel flash column chromatography using cold Petroleum Ether/Ethyl Acetate (PE/EA) eluent (100:1 to 30:1) at −40°C to afford the product **2a**-**2t**, **3a**-**3t**.

General procedure for the catalytic PKR of racemic 1u-1y

A solution of *rac*-**1u**-**1y** (0.15 mmol, 1.0 equiv.) and catalyst **I** (10 mol %) in toluene (6.0 ml) was stirred at −78°C for 15 min, and then NBS (1.05 equiv.) was added. After stirring at −78°C for 24 hours, the reaction mixture was subjected to silica gel flash column chromatography using cold PE/EA eluent (80:1 to 10:1) to afford the product **2u**-**2y**, **3u**-**3y**.

General procedure for the catalytic PKR of racemic 1z-1ae

A solution of *rac*-**1z**-**1ae** (0.15 mmol, 1.0 equiv.) and catalyst **I** (10 mol %) in toluene (6.0 ml) was stirred at −60°C for 15 min, and then NBS (1.05 equiv.) was added. After stirring at −60°C for 12 hours, the reaction mixture was subjected to column chromatography using neutral alumina or silica gel with cold PE/EA eluent (50:1 to 10:1) to afford the product **2z**-**2ae**, **3z**-**3ae**.

Supplementary Materials

This PDF file includes:
Sections S1 to S11
Figs. S1 to S32
Tables S1 and S2
References

REFERENCES AND NOTES

1. S. P. Roche, J. A. Porco Jr., Dearomatization strategies in the synthesis of complex natural products. *Angew. Chem. Int. Ed.* **50**, 4068–4093 (2011).

2. S.-L. You, *Asymmetric Dearomatization Reactions* (Wiley-VCH: Weinheim, 2016).

3. C.-X. Zhuo, W. Zhang, S.-L. You, Catalytic asymmetric dearomatization reactions. *Angew. Chem. Int. Ed.* **51**, 12662–12686 (2012).

4. W.-T. Wu, L. Zhang, S.-L. You, Catalytic asymmetric dearomatization (CADA) reactions of phenol and aniline derivatives. *Chem. Soc. Rev.* **45**, 1570–1580 (2016).

5. Z.-L. Xia, Q.-F. Xu-Xu, C. Zheng, S.-L. You, Chiral phosphoric acid-catalyzed asymmetric dearomatization reactions. *Chem. Soc. Rev.* **49**, 286–300 (2020).

6. J. C. C. Atherton, S. Jones, Diels-Alder reactions of anthracene, 9-substituted anthracenes and 9,10-disubstituted anthracenes. *Tetrahedron* **59**, 9039–9057 (2003).

7. R. Remy, C. G. Bochet, Arene-alkene cycloaddition. *Chem. Rev.* **116**, 9816–9849 (2016).

8. W. C. Wertjes, E. H. Southgate, D. Sarlah, Recent advances in chemical dearomatization of nonactivated arenes. *Chem. Soc. Rev.* **47**, 7996–8017 (2018).

9. C.-X. Zhuo, C. Zheng, S.-L. You, Transition-metal-catalyzed asymmetric allylic dearomatization reactions. *Acc. Chem. Res.* **47**, 2558–2573 (2014).

10. C. Zheng, S.-L. You, Catalytic asymmetric dearomatization by transition-metal catalysis: A method for transformations of aromatic compounds. *Chem* **1**, 830–857 (2016).

11. C. Zheng, S.-L. You, Catalytic asymmetric dearomatization (CADA) reaction-enabled total synthesis of indole-based natural products. *Nat. Prod. Rep.* **36**, 1589–1605 (2019).

12. F.-T. Sheng, J.-Y. Wang, W. Tan, Y.-C. Zhang, F. Shi, Progresses in organocatalytic asymmetric dearomatization reactions of indole derivatives. *Org. Chem. Front.* **7**, 3967–3998 (2020).

13. N. Ortega, S. Urban, B. Beiring, F. Glorius, Ruthenium NHC catalyzed highly asymmetric hydrogenation of benzofurans. *Angew. Chem. Int. Ed.* **51**, 1710–1713 (2012).

14. S. Zhu, D. W. C. MacMillan, Enantioselective copper-catalyzed construction of aryl pyrroloindolines via an arylation-cyclization cascade. *J. Am. Chem. Soc.* **134**, 10815–10818 (2012).

15. N. Dong, X. Li, F. Wang, J.-P. Cheng, Asymmetric Michael-Aldol tandem reaction of 2-substituted benzofuran-3-ones and enones: A facile synthesis of griseofulvin analogues. *Org. Lett.* **15**, 4896–4899 (2013).

16. Y.-C. Zhang, J.-J. Zhao, F. Jiang, S.-B. Sun, F. Shi, Organocatalytic asymmetric arylative dearomatization of 2,3-disubstituted indoles enabled by tandem reactions. *Angew. Chem. Int. Ed.* **53**, 13912–13915 (2014).

17. Z. Li, Y. Shi, Chiral phosphine oxide-Sc(OTf)$_3$ complex catalyzed enantioselective bromoaminocyclization of 2-benzofuranylmethyl N-tosylcarbamates. Approach to a novel class of optically active spiro compounds. *Org. Lett.* **17**, 5752–5755 (2015).

18. Q. Tian, J. Bai, B. Chen, G. Zhang, Chromium-catalyzed asymmetric dearomatization addition reactions of halomethyl heteroarenes. *Org. Lett.* **18**, 1828–1831 (2016).

19. D. Janssen-Müller, M. Fleige, D. Schlüns, M. Wollenburg, C. G. Daniliuc, J. Neugebauer, F. Glorius, NHC-catalyzed enantioselective dearomatizing hydroacylation of benzofurans and benzothiophenes for the synthesis of spirocycles. *ACS Catal.* **6**, 5735–5739 (2016).

20. R. Jiang, L. Ding, C. Zheng, S.-L. You, Iridium-catalyzed Z-retentive asymmetric allylic substitution reactions. *Science* **371**, 380–386 (2021).

21. J. E. Spangler, H. M. L. Davies, Catalytic asymmetric synthesis of pyrroloindolines via a rhodium(II)-catalyzed annulation of indoles. *J. Am. Chem. Soc.* **135**, 6802–6805 (2013).

22. Q. Cheng, H.-J. Zhang, W.-J. Yue, S.-L. You, Palladium-catalyzed highly stereoselective dearomative [3 + 2] cycloaddition of nitrobenzofurans. *Chem* **3**, 428–436 (2017).

23. Q. Cheng, F. Zhang, Y. Cai, Y.-L. Guo, S.-L. You, Stereodivergent synthesis of tetrahydrofuroindoles through Pd-catalyzed asymmetric dearomative formal [3 + 2] cycloaddition. *Angew. Chem. Int. Ed.* **57**, 2134–2138 (2018).

24. H. Wang, J. Zhang, Y. Tu, J. Zhang, Phosphine-catalyzed enantioselective dearomative [3 + 2] cycloaddition of 3-nitroindoles and 2-nitrobenzofurans. *Angew. Chem. Int. Ed.* **58**, 5422–5426 (2019).

25. Z. Lin, Y. Xue, X.-W. Liang, J. Wang, S. Lin, J. Tao, S.-L. You, W. Liu, Oxidative indole dearomatization for asymmetric furoindoline synthesis by a flavin-dependent monooxygenase involved in the biosynthesis of bicyclic thiopeptide thiostrepton. *Angew. Chem. Int. Ed.* **60**, 8401–8405 (2021).

26. Q. Wan, J.-H. Xie, C. Zheng, Y.-F. Yuan, S.-L. You, Silver-catalyzed asymmetric dearomatization of electron-deficient heteroarenes via interrupted Barton–Zard reaction. *Angew. Chem. Int. Ed.* **60**, 19730–19734 (2021).

27. Z.-P. Yang, R. Jiang, C. Zheng, S.-L. You, Iridium-catalyzed intramolecular asymmetric allylic alkylation of hydroxyquinolines: Simultaneous weakening of the aromaticity of two consecutive aromatic rings. *J. Am. Chem. Soc.* **140**, 3114–3119 (2018).

28. H.-F. Tu, P. Yang, Z.-H. Lin, C. Zheng, S.-L. You, Time-dependent enantiodivergent synthesis via sequential kinetic resolution. *Nat. Chem.* **12**, 838–844 (2020).

29. J. A. Carmona, C. Rodríguez-Franco, R. Fernández, V. Hornillos, J. M. Lassaletta, Atroposelective transformation of axially chiral (hetero)biaryls. From desymmetrization to modern resolution strategies. *Chem. Soc. Rev.* **50**, 2968–2983 (2021).

30. J. K. Cheng, S.-H. Xiang, S. Li, L. Ye, B. Tan, Recent advances in catalytic asymmetric construction of atropisomers. *Chem. Rev.* **121**, 4805–4902 (2021).

31. C.-X. Liu, W.-W. Zhang, S.-Y. Yin, Q. Gu, S.-L. You, Synthesis of atropisomers by transition-metal-catalyzed asymmetric C–H functionalization reactions. *J. Am. Chem. Soc.* **143**, 14025–14040 (2021).

32. G.-J. Mei, W. L. Koay, C.-Y. Guan, Y. Lu, Atropisomers beyond the C–C axial chirality: Advances in catalytic asymmetric synthesis. *Chem* **8**, 1855–1893 (2022).

33. W. Qin, Y. Liu, H. Yan, Enantioselective synthesis of atropisomers via vinylidene ortho-quinone methides (VQMs). *Acc. Chem. Res.* **55**, 2780–2795 (2022).

34. B. Wu, J. R. Parquette, T. V. RajanBabu, Regiodivergent ring opening of chiral aziridines. *Science* **326**, 1662 (2009).

35. J. R. Dehli, V. Gotor, Parallel kinetic resolution of racemic mixtures: A new strategy for the preparation of enantiopure compounds? *Chem. Soc. Rev.* **31**, 365–370 (2002).

36. L.-a. Liao, F. Zhang, O. Dmitrenko, R. D. Bach, J. M. Fox, A reactivity/affinity switch for parallel kinetic resolution: α-Amino acid quasienantiomers and the resolution of cyclopropene carboxylic acids. *J. Am. Chem. Soc.* **126**, 4490–4491 (2004).

37. I. Kreituss, J. W. Bode, Flow chemistry and polymer-supported pseudoenantiomeric acylating agents enable parallel kinetic resolution of chiral saturated N-heterocycles. *Nat. Chem.* **9**, 446–452 (2017).

38. Y.-C. Zhu, Y. Li, B.-C. Zhang, F.-X. Zhang, Y.-N. Yang, X.-S. Wang, Palladium-catalyzed enantioselective C−H olefination of diaryl sulfoxides through parallel kinetic resolution and desymmetrization. *Angew. Chem. Int. Ed.* **57**, 5129–5133 (2018).

39. A. G. Doyle, E. N. Jacobsen, Small-molecule H-bond donors in asymmetric catalysis. *Chem. Rev.* **107**, 5713–5743 (2007).

40. D. W. C. MacMillan, The advent and development of organocatalysis. *Nature* **455**, 304–308 (2008).

41. B. List, *Asymmetric Organocatalysis vol. 291 of Topics in Current Chemistry* (Springer, 2009).

42. S. Bertelsen, K. A. Jørgensen, Organocatalysis—after the gold rush. *Chem. Soc. Rev.* **38**, 2178–2189 (2009).

43. C. E. Song, *Cinchona Alkaloids in Synthesis and Catalysis: Ligands, Immobilization and Organocatalysis* (Wiley-VCH, 2009).

44. R. J. Ross, R. Jeyaseelan, M. Lautens, Rhodium-catalyzed intermolecular cyclopropanation of benzofurans, indoles, and alkenes via cyclopropene ring opening. *Org. Lett.* **22**, 4838–4843 (2020).

45. J. Carreras, M. Patil, W. Thiel, M. Alcarazo, Exploiting the π-acceptor properties of carbene-stabilized phosphorus centered trications [L₃P] ³⁺: Applications in Pt(II) catalysis. *J. Am. Chem. Soc.* **134**, 16753–16758 (2012).

46. F. Zhan, G. Liang, Formation of enehydrazine intermediates through coupling of phenyl-hydrazines with vinyl halides: Entry into the fischer indole synthesis. *Angew. Chem. Int. Ed.* **52**, 1266–1269 (2013).

47. J. Takagi, K. Takahashi, T. Ishiyama, N. Miyaura, Palladium-catalyzed cross-coupling reaction of bis(pinacolato)diboron with 1-alkenyl halides or triflates: Convenient synthesis of unsymmetrical 1,3-dienes via the borylation-coupling sequence. *J. Am. Chem. Soc.* **124**, 8001–8006 (2002).

48. W. Liu, H. J. Lim, T. V. RajanBabu, Asymmetric hydrovinylation of vinylindoles. A facile route to cyclopenta[g]indole natural products (+)-*cis*-trikentrin A and (+)-*cis*-trikentrin B. *J. Am. Chem. Soc.* **134**, 5496–5499 (2012).

49. J. Ma, Y. Fu, E. Dmitrieva, F. Liu, H. Komber, F. Hennersdorf, A. A. Popov, J. J. Weigand, J. Liu, X. Feng, Helical nanographenes containing an azulene unit: Synthesis, crystal structures, and properties. *Angew. Chem. Int. Ed.* **59**, 5637–5642 (2020).

50. S. Huang, H. Wen, Y. Tian, P. Wang, W. Qin, H. Yan, Organocatalytic enantioselective construction of chiral azepine skeleton bearing multiple-stereogenic elements. *Angew. Chem. Int. Ed.* **60**, 21486–21493 (2021).

51. Y. Liu, X. Wu, S. Li, L. Xue, C. Shan, Z. Zhao, H. Yan, Organocatalytic atroposelective intramolecular [4+2] cycloaddition: Synthesis of axially chiral heterobiaryls. *Angew. Chem. Int. Ed.* **57**, 6491–6495 (2018).

52. K. Vermeulen, D. R. Van Bockstaele, Z. N. Berneman, The cell cycle: A review of regulation, deregulation and therapeutic targets in cancer. *Cell Prolif.* **36**, 131–149 (2003).

53. T. Otto, P. Sicinski, Cell cycle proteins as promising targets in cancer therapy. *Nat. Rev. Cancer* **17**, 93–115 (2017).

54. M. J. Frisch, G. W. Trucks, H. B. Schlegel, G. E. Scuseria, M. A. Robb, J. R. Cheeseman, G. Scalmani, V. Barone, B. Mennucci, G. A. Petersson, H. Nakatsuji, M. Caricato, X. Li, H. P. Hratchian, A. F. Izmaylov, J. Bloino, G. Zheng, J. L. Sonnenberg, M. Hada, M. Ehara, K. Toyota, R. Fukuda, J. Hasegawa, M. Ishida, T. Nakajima, Y. Honda, O. Kitao, H. Nakai, T. Vreven, J. A. Montgomery Jr., J. E. Peralta, F. Ogliaro, M. Bearpark, J. J. Heyd, E. Brothers, K. N. Kudin, V. N. Staroverov, T. Keith, R. Kobayashi, J. Normand, K. Raghavachari, A. Rendell, J. C. Burant, S. S. Iyengar, J. Tomasi, M. Cossi, N. Rega, J. M. Millam, M. Klene, J. E. Knox, J. B. Cross, V. Bakken, C. Adamo, J. Jaramillo, R. Gomperts, R. E. Stratmann, O. Yazyev, A. J. Austin, R. Cammi, C. Pomelli, J. W. Ochterski, R. L. Martin, K. Morokuma, V. G. Zakrzewski, G. A. Voth, P. Salvador, J. J. Dannenberg, S. Dapprich, A. D. Daniels, Ö. Farkas, J. B. Foresman, J. V. Ortiz, J. Cioslowski, D. J. Fox, Gaussian 09, Revision D.01, Gaussian Inc., Wallingford CT, 2013.

55. A. V. Marenich, C. J. Cramer, D. G. Truhlar, Universal solvation model based on solute electron density and on a continuum model of the solvent defined by the bulk dielectric constant and atomic surface tensions. *J. Phys. Chem. B* **113**, 6378–6396 (2009).

56. Y. Zhao, D. G. Truhlar, The M06 suite of density functionals for main group thermochemistry, thermochemical kinetics, noncovalent interactions, excited states, and transition elements: Two new functionals and systematic testing of four M06-class functionals and 12 other functionals. *Theor. Chem. Acc.* **120**, 215–241 (2008).

57. F. Weigend, R. Ahlrichs, Balanced basis sets of split valence, triple zeta valence and quadruple zeta valence quality for H to Rn: Design and assessment of accuracy. *Phys. Chem. Chem. Phys.* **7**, 3297–3305 (2005).

58. R. Krishnan, J. S. Binkley, R. Seeger, J. A. Pople, Self-consistent molecular orbital methods XX. A basis set for correlated wave functions. *J. Chem. Phys.* **72**, 650–654 (1980).

59. C. Y. Legault, CYLview, version 1.0b; Université de Sherbrooke (2009); www.cylview.org.

60. R. F. W. Bader, A quantum theory of molecular structure and its applications. *Chem. Rev.* **91**, 893–928 (1991).

61. T. Lu, F. Chen, Multiwfn: A multifunctional wavefunction analyzer. *J. Comput. Chem.* **33**, 580–592 (2012).